

Available online at www.sciencedirect.com

ScienceDirect

journal homepage: www.elsevier.com/locate/AJPS

Original Research Paper

Spatiotemporally co-delivery of triple therapeutic drugs via HA-coating nanosystems for enhanced immunotherapy



Chaoqun Ma, Yichao Duan, Chaohui Wu, Erjuan Meng, Pingping Li, Zhenzhong Zhang, Chunhua Zang*, Xueling Ren*

Key Laboratory of Targeting Therapy and Diagnosis for Critical Diseases, School of Pharmaceutical Science, Zhengzhou University, Zhengzhou 450001, China

ARTICLE INFO

Article history:

Received 15 April 2021

Revised 13 July 2021

Accepted 28 July 2021

Available online 21 August 2021

Keywords:

Hyaluronic acid

PD-L1

Immunogenic cell death

Immunotherapy

ABSTRACT

There is growing empirical evidence that certain types of chemotherapy and phototherapy trigger immunogenic cell death and enhance the therapeutic anticancer efficacy of genetic immunotherapy. However, the main challenge is spatiotemporally co-delivering different drugs to maximize the therapeutic index of the combination therapy. In this study, a drug delivery system (HTCP-Au/shPD-L1/DOX) was designed with a polysaccharide-wrapped shell and a condensed DNA core. To construct the HTCP-Au vector, dodecyl side chains with a polyethylenimine (PEI) head were grafted onto hyaluronic acid, and AuNPs were grafted via Au-S bonds. During drug loading, PEI arrested shRNA plasmid DNA targeting programmed cell death ligand 1 (shPD-L1) via electrostatic interactions. It also formed a PEI-DNA core that was automatically enclosed when aliphatic hydrocarbons pulled the hyaluronic acid backbone. A hydrophobic interlayer consisting of dodecyl bridge chains between the PEI-DNA core and the hyaluronic acid shell was required to accommodate hydrophobic doxorubicin. *In vitro* and *in vivo* assays demonstrated that this core-shell drug delivery system could efficiently load and transport three different drugs and effectively target tumors. Moreover, it could activate the immune system, thereby providing promising therapeutic efficacy against tumor growth and metastasis.

© 2021 Shenyang Pharmaceutical University. Published by Elsevier B.V.

This is an open access article under the CC BY-NC-ND license

(<http://creativecommons.org/licenses/by-nc-nd/4.0/>)

1. Introduction

Cancer is a major culprit affecting human health, and the imperative in the development of cancer treatment is improving efficacy while reducing toxicity. Over the past

decades, genetic immunotherapy, which intervenes in host immunity by using genetic technology to recognize and eradicate cancer cells, has attracted widespread research attention [1–3]. However, the dismal objective response rates of immune system targeted therapies are less than ideal, which may be attributed partly to the heterogeneity of

* Corresponding authors.

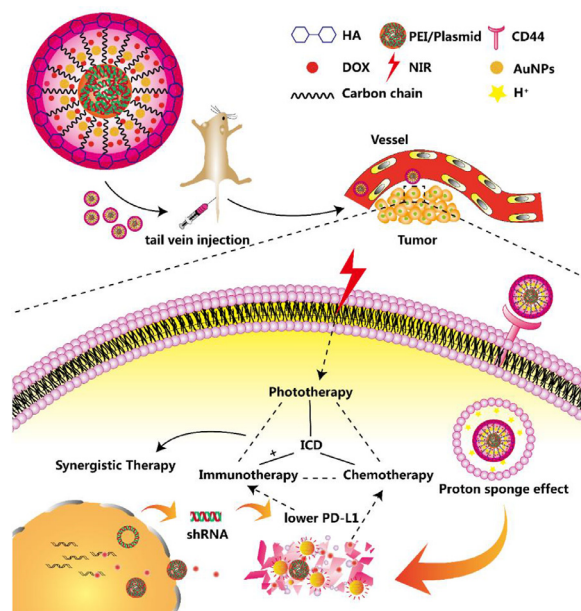
E-mail addresses: 1835782801@qq.com (C.H. Zang), renxueling@zzu.edu.cn (X.L. Ren).

Peer review under responsibility of Shenyang Pharmaceutical University.

cancer and the incomplete activation of immune system [4–6]. Recently, it has been discovered that some specific treatments, such as chemotherapy and phototherapy, can enhance the curative effect of genetic immunotherapy by triggering a special cell death called immunogenic cell death (ICD) or activating the adaptive immune response system [7–10]. Therefore, combining different localized treatments and genetic immunotherapy can achieve a promising therapeutic effect against cancer [11]. Nevertheless, the therapeutic agents used in immunogenetic therapy, chemotherapy, and phototherapy differ vastly in terms of their molecular structures and/or physicochemical properties. Hence, it is crucial to spatiotemporally co-deliver these distinct agents to maximize the therapeutic index and elicit responses that cannot be achieved with any of the agents alone.

Hyaluronic acid (HA) is a natural linear polysaccharide represented by alternating D-glucuronic acid and N-acetyl glucosamine units. In last decades, HA-based nanoparticles have attracted great attention in drug- and gene-delivery due to its excellent biocompatibility, biodegradability, wonderful modification, and tumor-targeting ability [12–14]. In general, HA has poor capacity for loading nucleic acid because of its electro-negativities. To overcome this obstacle, HA usually be modified with highly positively charged functional groups, such as polyethylenimine (PEI) [15,16]. The cationic modification can improve the capacity for nucleic acid loading but shorten *in vivo* circulation because of nonspecific interactions between particles and serum proteins. More concerning, the compressed structure of the complexes will be detrimental to foreign drug loading when cationic HA interact with nucleic acid. To highlight strengths and circumvent weaknesses, an HA-based nanoparticle with core-shell structure was designed and constructed to achieve synergistic spatiotemporal drug delivery in this study. As shown in Scheme 1, PEI was hung off the HA main structure through a carbon bridge chain instead of directly linking to HA in this study. When loaded with nucleic acid-based drugs for genetic immunotherapy, PEI arrested DNA by forming the PEI/DNA kernel through electrostatic interaction. HA was simultaneously driven by dodecyl chains and PEI and automatically wrapped around PEI/DNA to form a shell. In addition, there was a hydrophobic intermediate layer formed by the long alkyl chain between the PEI/DNA core and the HA shell, which provided the space necessary to accommodate other drugs. This core-shell nano-drug delivery system uses the electronegativity of the HA shell to avoid clearance by the reticuloendothelial system, prolongs *in vivo* circulation, and utilizes the effects of HA and CD44 on tumor cell surfaces to achieve synergistic, targeted drug delivery.

As a major target of antitumor genetic immunotherapy, programmed cell death ligand 1 (PD-L1) is expressed on the surfaces of various tumor cells and plays a key role in tumor immune evasion [17]. It has been shown that silencing PD-L1 expression by RNA interference (RNAi) can reactivate the T-cell based immune response, resulting in the detection and elimination of tumor cells [18,19]. Doxorubicin (DOX), an inhibitor of DNA and RNA biosynthesis, is commonly used as a chemotherapeutic drug for clinical tumor treatment. In particular, DOX can trigger ICD and enhance the immunomodulation effects of



Scheme 1 – Schematic diagram of drug delivery and anti-tumor mechanism of HTCP-Au/shPD-L1/DOX nanoparticles.

PD-L1-based immunotherapy [5,20–23]. Equally attractive is that apart from the immunomodulatory effects of DOX, gold nanoparticles (AuNPs), widely used in photodynamic therapy, have been found to stimulate the immune system [10,24]. Therefore, a combination of RNAi silencing PD-L1 (shPD-L1), DOX, and AuNPs may be an effective strategy to improve immunogenetic antitumor efficacy and can be used as a model drug combination to clarify the effect of a core-shell, multi-drugs co-delivery system.

In this study, we first grafted AuNPs on HTCP to construct HTCP-Au. Then, the shPD-L1 and DOX were loaded in turn to form the antitumor drug delivery system, HTCP-Au/shPD-L1/DOX, with a core-shell structure. Moreover, we explored and validated the antitumor effectiveness and safety of this novel drug delivery system (HTCP-Au/shPD-L1/DOX), both *in vitro* and *in vivo*. Based on this study, we expect to achieve the convergence of different localized treatments and genetic immunotherapy and provide more effective interventions in cancer therapy.

2. Materials and methods

2.1. Materials

Hyaluronic acid (HA; MW = 200–400 kDa) was purchased from Bloomage Freda Biopharm Corporation (Shandong, China). The 1-(3-(dimethylamino)propyl)-3-ethylcarbodiimide hydrochloride (EDC), N-hydroxysuccinimide (NHS), and polyethylenimine (PEI; MW = 600 Da) were purchased from Aladdin Bio-Chem Technology Co. (Shanghai, China). The 12-aminododecanoic acid was purchased from Yuanye Bio-Technology Corporation (Shanghai, China). L-Cys- was purchased from Macklin Biochemical Corporation

(Shanghai, China). Chloroauric acid was purchased from Zhanyun Chemical Corporation (Shanghai, China). DOX was purchased from Aladdin Bio-Chem Technology Co. (Shanghai, China). The 3-(4,5-dimethyl-2-thiazolyl)-2,5-diphenyl-2-H-tetrazolium bromide (MTT) was purchased from Solarbio Science and Technology Corporation (Beijing, China). Fluorescein isothiocyanate (FITC) fluorescent probe was purchased from Sigma-Aldrich Corp. (St. Louis, MO, USA). LysoRed lysosome probe, and cell apoptosis and cycle testing kits were purchased from KeyGen Biotech Corporation (Nanjing, China). TRIzol reagent was purchased from CoWin Bioscience (Jiangsu, China). The enzyme-linked immunosorbent assay (ELISA) kit was purchased from Winter Song Boye Biotechnology Corporation (Beijing, China). The RNAi negative control plasmid (shNC), and PD-L1 targeting RNAi plasmid (shPD-L1) were purchased from GenePharma Pharmaceutical Technology Co. Ltd. (Shanghai, China). The target sequence against PD-L1 was 5'-GAG ACG TAA GCA GTG TTG AA-3'. The 4T1 mouse breast cancer cells were purchased from the Cell Bank of the Chinese Academy of Science (Shanghai, China).

2.2. Preparation of HTCP-Au

2.2.1. HTCP preparation

HA was activated by the classical EDC-NHS method [25–27]. In short, 0.1500 g HA, 0.0690 g EDC, and 0.0420 g NHS were dissolved in 15 ml formamide solution and stirred at 20–25 °C under nitrogen protection for 4 h. Then, 0.1800 g of 12-aminododecanoic acid was added to the above mixture and stirred in the dark at room temperature for 48 h to generate HA-C₁₂. Then 0.1510 g L-Cys was activated by a similar EDC-NHS approach and reacted with 0.2500 g HA-C₁₂ under nitrogen protection for 5 h to generate HA-C-Cys. After being dialyzed and lyophilized, 0.1500 g HA-C-Cys dissolved in 15 ml boric acid buffer (pH 9.11) was mixed with 0.5000 g PEI in 400 μl HCl (3.7%, v/v) to generate HTCP. The mixture was stirred at room temperature in the dark under nitrogen protection for 48 h. The final product (HTCP) was dialyzed against ultrapure water for 2 d and obtained by lyophilization at 43.67% yield.

2.2.2. AuNP preparation

AuNPs were prepared by the citric acid reduction method [28–31]. In short, 5 ml fresh trisodium citrate solution (1%, w/v) was added to 95 ml boiled auric acid solution (0.01%, w/v). The mixture was rapidly stirred until the color of the reaction system changed from light yellow to wine red and remained stable for 5 min. The AuNP solution was obtained by stirring the mixture until it naturally cooled to room temperature. The yield was 81.76%.

2.2.3. HTCP-Au preparation and characterization

As previously reported [31–33], HTCP (0.5000 g) was dissolved in 90 mL ultrapure water, and 90 ml AuNP solution was added dropwise under nitrogen protection. The mixture was stirred in the dark for 24 h and then centrifuged at 1.2×10^4 r/min for 20 min. The supernatant was discarded, and the precipitate was washed thrice in ultrapure water to obtain the target product, HTCP-Au.

The chemical structure of the final product (HTCP-Au) was characterized by nuclear magnetic resonance imaging (¹H NMR; Avance III-400, Bruker GmbH, Karlsruhe, Germany). Elemental analysis was conducted by X-ray energy dispersive spectroscopy (EDS; AXIS Supra X, Shimadzu Corp., Kyoto, Japan). Photothermal conversion activity was evaluated with a thermal imager (Ti25; Fluke Corp., Everett USA). Particle size and zeta potential were determined by dynamic light scattering (DLS; Nano-ZS90, Malvern Instruments, Malvern, UK).

2.3. Preparation and characterization of nano drug delivery system for combination therapy (HTCP-Au/shPD-L1/DOX)

To form HTCP-Au/shPD-L1, the shPD-L1 solution was added to the nanoparticle HTCP-Au aqueous solutions at a mass ratio of 1:3, and the mixture was vortexed for 30 s and then incubated at room temperature for 30 min. Then, DOX was added to the above mixture at different mass ratios ($W_{\text{HTCP-Au}} \cdot W_{\text{DOX}} = 0.2:1, 0.5:1, 1:1, 2.5:1, 5:1$), and was incubated at room temperature for 30 min to generate HTCP-Au/shPD-L1/DOX. After centrifugation at 1.2×10^4 r/min for 15 min, the supernatant was taken to determine the DOX content by fluorescence spectrophotometry. The drug-loading rate ($DL\% = C_1 / (C_1 + C_2) \times 100$) and encapsulation efficiency ($EE\% = C_1 / C_3 \times 100$) were calculated. C₁ is the mass of encapsulated drug, C₂ is the mass of HTCP-Au and shPD-L1, C₃ is the mass of added drug.

To detect the release of DOX, HTCP-Au/shPD-L1/DOX was dispersed in phosphate-buffered saline (PBS, pH 6.5 or pH 6.0) or hydrochloric acid (pH 5.0, with 1% SDS) and placed in a constant temperature rocker rotator at 37 °C, 50 r/min. As for the NIR irradiation group, the samples were irradiated with an 808 nm laser (1.5 W/cm²) for about 30 s. At 0.5, 1, 2, 4, 8, 12, 24, 36 and 48 h, samples were removed from the system to be tested, and an equal volume of solvent was added. Fluorescence intensity was detected and cumulative release was calculated.

Agarose gel electrophoresis was used to detect the interaction between HTCP-Au and nucleic acid shPD-L1. DLS was used to determine the particle size and zeta potential of HTCP-Au/shPD-L1/DOX and transmission electron microscopy (TEM; TecnaiF20, FEI, Hillsboro, OR, USA) was used for its morphological characterization.

2.4. Cellular uptake

Firstly, HTCP-Au was labeled by FITC. In short, 0.0100 g FITC and 0.0042 g N, N'-Carbonyldiimidazole were dissolved in 10 ml DMSO, and stirred under nitrogen protection for 4 h. 0.0050 g HTCP-Au was added to the above mixture and stirred under nitrogen protection for 24 h to generate HTCP-Au-FITC. Then, HTCP-Au-FITC was used to generate HTCP-Au-FITC/shNC in a method similar to the preparation of HTCP-Au/shNC.

The 4T1 mouse breast cancer cells in logarithmic growth phase were seeded in 12-well plates at a density of 1.5×10^5 cells/well and incubated overnight. The medium was removed and replaced with medium containing FITC-labeled

HTCP-Au/shNC (HTCP-Au-FITC/shNC, 100 µg/ml). After 2, 4 and 6 h continuous culture, the medium was discarded, the cells were washed twice with PBS, and cell uptake efficiency was detected by flow cytometry (FCM; Accuri C6, BD Biosciences, Franklin Lakes, NJ, USA).

HTCP-Au-FITC and HTCP-Au-FITC/shNC were added to 4T1 cells in logarithmic growth phase. After 6 h continuous culture, the medium was discarded, the cells were washed thrice with PBS, and medium containing lysosome fluorescent probe was added. After 40 min, the cells were washed thrice with PBS and 1 ml 4% paraformaldehyde was added. After 15 min fixation, cells were washed thrice with PBS and 1 ml medium containing DAPI was added. After 15 min, the medium was discarded, the cells were washed thrice with PBS and observed by fluorescence microscopy (IX53, Olympus Corp., Tokyo, Japan).

2.5. Cell proliferation

The 4T1 cells were seeded in a 96-well plate at a density of 3.0×10^3 cells/well and cultured conventionally for 16 h. The old medium was removed and replaced with new media containing various drug administration systems. After 48 h incubation, the cell proliferation rate was detected by MTT assay ($n=5$). For laser irradiation groups, cells were irradiated by 808 nm laser after 6 h administration. The treatment groups were the PBS negative control group (NC), the phototherapy group with 808 nm laser irradiation (HTCP-Au/shNC-808), the chemotherapy group (HTCP-Au/shNC/DOX), the genetic immunotherapy group (HTCP-Au/shPD-L1), and the combination treatment group with 808 nm laser irradiation (HTCP-Au/shPD-L1/DOX-808). The dealing dose was composed of 10 µg/ml HTCP-Au, with or without shPD-L1 (3.3 µg/ml), DOX (4 µg/ml), and infrared 808-nm laser irradiation (1.5 W/cm², 60 s).

2.6. Cell cycle and apoptosis

The cell cycle of the 4T1 cells induced by HTCP-Au/shPD-L1/DOX-808 was analyzed by FCM after the cells were stained with propidium iodide (PI), according to the manufacturer's protocol for the cell cycle detection kit. Apoptosis of the treated cells was detected using the Annexin V-FITC/PI double staining apoptosis kit as standard operational procedure. The cells received either PBS, HTCP-Au/shNC-808, HTCP-Au/shNC/DOX, or HTCP-Au/shPD-L1 (the same mass ratio of $W_{\text{HTCP-Au}}:W_{\text{DNA}}:W_{\text{DOX}}$ to be 15:5:6) as the control groups.

2.7. Xenograft tumor mouse model

Female BALB/c mice (16–20 g, 4 weeks old) were provided by the Henan Laboratory Animal Center (Henan, China). All animal experiments were conducted in accordance with the National Regulation on the Management of Laboratory Animals and approved by the Ethics Committee of Zhengzhou University. The 4T1 tumor cells were absorbed into a single-cell suspension and subcutaneously injected into the right forelimb of mice at 10^6 cells/0.2 ml. When the tumor volumes reached $\sim 100 \text{ mm}^3$, the mice were used for further experiments.

2.8. In vivo biodistribution and photothermal conversion

IR783 or IR783-labeled HTCP-Au/shNC was injected into the tail veins of 4T1 tumor-bearing mice and *in vivo* imaging was performed at predetermined times (1, 3, 5, 7, 12 and 24 h). Finally, the mice were sacrificed, and the major organs (heart, liver, spleen, lung, and kidney) and tumors were excised and examined by fluorescence imaging (In-Vivo FX PRO; Bruker GmbH, Karlsruhe, Germany).

A single dose of HTCP-Au/shNC (15 mg/kg HTCP-Au and 5 mg/kg shNC) was injected into tumor-bearing mice via the caudal vein. Five hours later, the tumor was irradiated with an 808 nm laser at 1.5 W for 30 s, and thermal imaging was recorded with an infrared thermal imager (Ti200, Fluke Corp., Everett, WA, USA).

2.9. In vivo antitumor efficacy

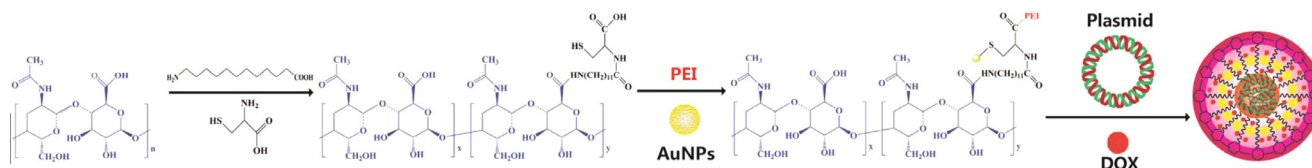
Mice harboring 4T1 tumors were randomly divided into six groups with five mice per group and were injected through the tail vein with saline, HTCP-Au/shNC, HTCP-Au/shNC-808, HTCP-Au/shNC/DOX, HTCP-Au/shPD-L1, and HTCP-Au/shPD-L1/DOX-808 (15 mg/kg HTCP-Au, 5 mg/kg shPD-L1, or shNC, 6 mg/kg DOX) every 6 days. For the mice of the HTCP-Au/shNC-808 and HTCP-Au/shPD-L1/DOX-808 groups, the tumor was irradiated for 30 s with near-infrared (NIR; 1.5 W/cm²), 5 h after the first injection, and every 3 d thereafter. The tumor volume and body weight were monitored every 2 d. On Day 13 after injection, the mice were sacrificed, and their tumor tissues were excised and weighed to calculate tumor inhibition rates. In addition, the tumor tissues were dewaxed, stained, dehydrated, rendered transparent, and sealed for histopathological and immunohistochemical analyses. The level of interferon gamma (IFN- γ) secretion was assayed using an enzyme-linked immunosorbent assay (ELISA) kit.

2.10. In vivo safety evaluation

Mouse weight changes, organ weight index, and routine blood tests were assessed to evaluate the safety profile of HTCP-Au/shPD-L1/DOX-808. Moreover, after the experiments, blood was collected from the retro-orbital sinus for the spectrophotometric measurement of aspartate aminotransferase (AST), lactate dehydrogenase (LDH), and creatine kinase (CK). The major organs including hearts, livers, spleens, lungs, and kidneys were excised for histopathological examination.

2.11. Real time quantitative polymerase chain reaction (qPCR)

Total RNA from tumor cells or tumor tissues was extracted using the TRIzol method and 2 µl RNA was used in reverse transcription (RT). qPCR amplification (T100™ Thermal Cycler, Bio-Rad Laboratories, Hercules, CA, USA) was performed with specific primers. Hypoxanthine Phosphoribosyltransferase (HPRT) mRNA was the internal reference. The PD-L1 primers were 5'-CTT TTC CTC TGC TCA GTG CCG-3' (upstream), and 5'-GAC CTC TGT GTT CCC TGC TTG-3' (downstream). The HPRT primers were 5'-CTC CGC



Scheme 2 – Preparation process of drug delivery system HTCP-Au/shPD-L1/DOX.

CGG CTT CCT CA-3' (upstream), and 5'-ACC TGG TTC ATC GCT AT-3' (downstream).

2.12. Western blot

Tumor tissues were digested with radioimmunoprecipitation assay (RIPA) lysis buffer to extract the proteins. The extracted proteins were quantitated using the bicinchoninic acid (BCA) method, and separated using sodium dodecyl sulfate polyacrylamide gel electrophoresis (SDS-PAGE). Proteins were then transferred onto a nitrocellulose membrane using the Trans-Blot Turbo Transfer System (Bio-Rad Laboratories, Hercules, CA, USA), and the transmembrane was conducted and sealed with 5% skimmed milk powder. Anti-PD-L1 (1:500) or anti- β -actin (1:1000) antibodies were added, and the transmembranes were incubated at 4°C overnight. The transmembranes were washed thrice in Tris buffer plus polysorbate 20 (TBST), treated with secondary antibody (1:3000), and incubated at room temperature for 30 min. After washing thrice with TBST, the target proteins were visualized using chemiluminescence and analyzed using ImageJ 1.52a software (NIH, Bethesda, MD, USA).

2.13. Statistical analysis

All data were given as mean \pm standard deviation (SD). One way analysis of variance was used to determine the significance of the difference. The differences were considered significant for * $P < 0.05$; ** $P < 0.01$; *** $P < 0.001$; **** $P < 0.0001$.

3. Results and discussion

3.1. HTCP-Au synthesis and characterization

Combined drug deliveries provide a greater possibility for the complete cure of tumors, but the key is how to deliver drugs with different structures and physicochemical properties. To this end, researchers have carried out a lot of work. In recent years, polysaccharides have shown great advantages in drug delivery. A modified shell of Ti_3C_2 nanosheets with mixed polysaccharides could enhance the tumor accumulation, biocompatibility, and immune activation of the drug delivery system, and achieve synergistic treatment with PTT, PDT, and chemotherapy. In this work, we designed and prepared a "core-shell" structured nano drug delivery system with hyaluronan polysaccharide to achieve the simultaneous delivery of a trio of antitumor drugs. As illustrated in

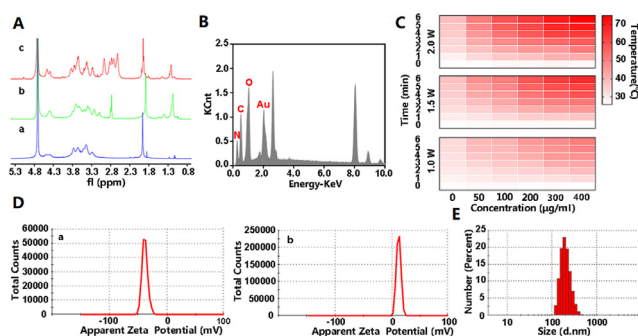


Fig. 1 – Characterization of synthesized HTCP-Au. (A) ^1H NMR spectra of HA (a), HA- C_{12} -Cys (b) and HTCP (c); (B) The EDS elemental analysis result of HTCP-Au; (C) The photothermal conversion effect of HTCP-Au with various irradiation (808 nm). (D) Zeta potential distribution of HA (a) and HTCP-Au (b). (E) Size of HTCP-Au.

Scheme 2, to construct a drug delivery carrier of HTCP-Au that can simultaneously load nucleic acids, chemicals, and gold nanoparticles, we grafted HA with 12-aminododecanoic acid and L-cysteine as bridge chains, and grafted small molecular weight PEI, using the sulfhydryl group of L-cysteine to connect gold nanoparticles.

Fig. 1 shows the structural characterization of HTCP-Au and its representative intermediates. The ^1H NMR results are shown in Fig. 1A. Compared with the raw material HA, the peaks at 1.0–1.6 ppm in the HA-C-Cys and HTCP spectra correspond to adipose chain methylenes. The peak at 2.8 ppm in the HA-C-Cys-spectrum was inferred to be the cysteine sulfhydryl peak. Hence, C_{12} and L-Cys were successfully coupled. The peak in the 2.5–3.0 ppm region of the HTCP spectrum corresponded to the PEI methylene. To elucidate HTCP-Au composition and structure, we conducted an elemental analysis by EDS (Fig. 1B). In the carrier HTCP-Au, the mass fractions of HA, PEI, and AuNPs were 53%, 21%, and 15%, respectively. The 808 nm laser irradiation increased the temperature of the HTCP-Au aqueous solution in a time-, dose-, and intensity-dependent relationship, which indicated that the HTCP-Au had good photothermal conversion activity (Fig. 1C). DLS was used to investigate the zeta potential changes and particle sizes of HTCP-Au. Fig. 1D and 1E show that the zeta potential of HA was -37.3 ± 1.37 mV, while that for HTCP-Au was 10.54 ± 0.41 mV. Therefore, the electropositive functional group PEI was successfully grafted. The HTCP-Au particle size was 232.3 ± 23.1 nm, and it provided

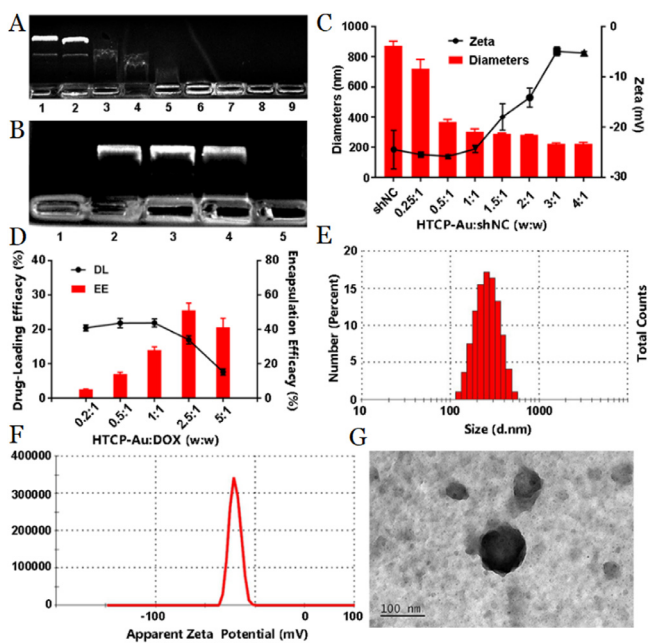


Fig. 2 – Characterization of synthesized HTCP-Au/shPD-L1/DOX. (A) Gel retardation assay of HTCP-Au/shNC at various mass ratios (lane 1–9: the HTCP-Au: shNC mass ratios of 0:1, 0.05:1, 0.1:1, 0.2:1, 0.5:1, 1:1, 2:1, 3:1, and 4:1 respectively); (B) Serum nuclease protection assay of HTCP-Au/shNC (lane 1: HTCP-Au/shNC; lane 2: shNC; lane 3: HTCP-Au/shNC treated with heparin; lane 4: HTCP-Au/shNC treated with heparin and serum; lane 5: shNC treated with serum); (C) Size and zeta potential of HTCP-Au/shNC at various mass ratios; (D) Drug-loading efficacy and encapsulation efficiency of HTCP-Au/shNC to DOX at different mass ratios; (E) Size distribution of HTCP-Au/shPD-L1/DOX; (F) Zeta potential distribution of HTCP-Au/shPD-L1/DOX; (G) TEM image of HTCP-Au/shPD-L1/DOX at a mass ratio of 15:5:6.

a structural basis for the formation of a nano drug delivery system.

3.2. HTCP-Au/shPD-L1/DOX preparation and characterization

For the drug delivery system HTCP-Au/shPD-L1/DOX with core-shell structure, the most noteworthy feature was that the redundant positive charges of PEI-DNA were cunningly covered in negative surface charges of HA, which reconciled with loading DNA and long *in vivo* circulation. We firstly detected the HTCP-Au nucleic acid loading capacity by agarose gel electrophoresis. With an increasing HTCP-Au:shNC mass ratio, the shNC migration rate gradually declined and the density of shNC bands slowly decreased (Fig. 2A). At a 1:1 mass ratio, shNC was completely blocked in the sampling hole, suggesting that HTCP-Au loaded the shNC completely at HTCP-Au:shNC mass ratios of up to 1:1. The protective effect of HTCP-Au on DNA is shown in Fig. 2B. No DNA band was found in the HTCP-Au/shNC group (lane 1), while shNC could

be released from HTCP-Au/shNC by heparin addition (lane 3), and its mobility was consistent with that of free shNC (lane 2). The shNC band disappeared (lane 5) due to the degradation of nucleic acid by serum. Taking a different approach, the presence of HTCP-Au deactivated shNC degradation by serum and the shNC band was visible (lane 4). The results of the agarose gel test demonstrate that HTCP-Au can not only effectively load DNA but also protect DNA from degradation in serum.

As reported, when cationic PEI-modified polysaccharides, such as PEI-modified laminarin [34], interacted with nucleic acid to produce nanoparticles, the zeta potential of the complexes changed regularly. When cationic carriers were precisely and completely loaded with anionic DNA, the positive and negative charges were balanced and the zeta potential of carriers/DNA nanoparticles was approximately zero. When the carrier content was increased, and exceeded, the zeta potential of the nanoparticles became positive due to the redundant positive charges of cationic carriers. In this study, the zeta potential of HTCP-Au alone was positive (10.54 ± 0.41 mV). However, the zeta potential of HTCP-Au/shNC remained negative, not positive, even when HTCP-Au was in excess and the HTCP-Au/shNC mass ratio was up to 4:1 (Fig. 2C). These results were consistent with our hypothesis that shNC is condensed by PEI and the redundant positive charges of PEI-shNC was cunningly covered in an anionic HA coating. In addition, Fig. 2C shows that the free shNC particle size was 871.5 ± 54.8 nm, and the particle sizes of HTCP-Au/shNC shrank and stabilized at 222.4 ± 11.9 nm with the increase of HTCP-Au concentration. Based on the foregoing results, the HTCP-Au:DNA mass ratio was set to 3:1 for the following experiments.

It has been demonstrated that DOX could inhibit cell proliferation by inserting into DNA double strands [35]. Therefore, DOX loading was performed after HTCP-Au/shNC preparation, which was beneficial to restrict DOX in the self-assembled hydrophobic interlayer composed of alkane bridge chains between the HA shell and the PEI/shNC core. Fig. 2D shows that the drug encapsulation efficiency of HTCP-Au/shNC/DOX gradually increased and reached a maximum value of $51.07\% \pm 4.23\%$ with a fixed DOX concentration and an HTCP-Au:DOX mass ratio up to 2.5:1. At that point, the DOX-loading rate reached $16.96\% \pm 1.17\%$. The particle size and zeta potential of HTCP-Au/shPD-L1/DOX were 243.2 ± 32.8 nm and -19.9 ± 0.8 mV, respectively (Fig. 2E and 2F). Furthermore, TEM images clearly demonstrated that HTCP-Au/shNC/DOX nanoparticles were roughly spherical (Fig. 2G).

The DOX release profile was investigated with simulated conditions of tumor microenvironment (pH 6.5), tumor cell (pH 6.0), and lysosome (pH 5.0). Results showed that the release of DOX was fastest at pH 5.0, which may be due to the proton sponge effect induced by cationic PEI. It has been reported [36] that a photo-responsive drug delivery system has the potential to promote drug release under laser irradiation; therefore, we set a group with 808 nm laser irradiation. However, results showed little effect of laser irradiation on DOX release, which might be due to the small dose of irradiation (Fig. S1).

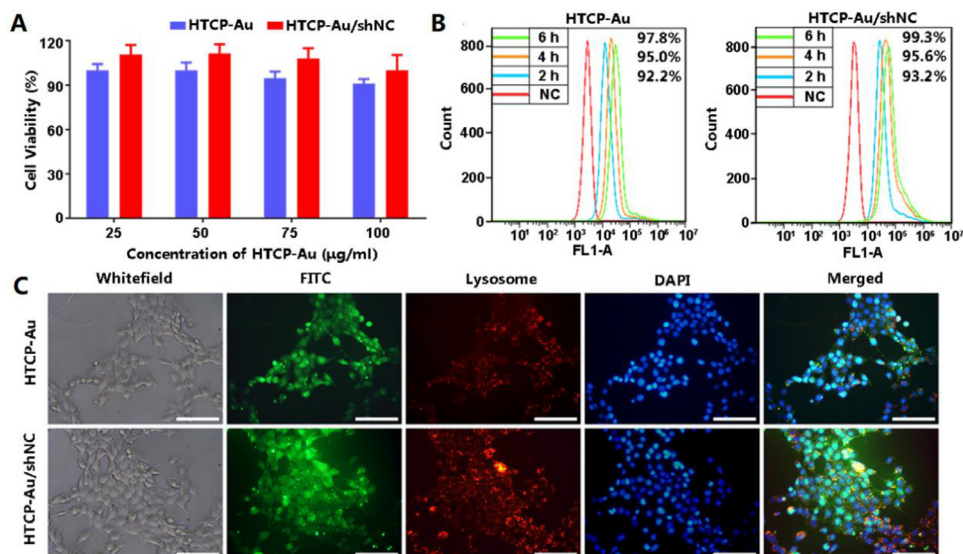


Fig. 3 – Toxicity and cellular uptake of HTCP-Au. (A) Cell viability of 4T1 cells after treatment with HTCP-Au and HTCP-Au/shNC for 48 h; **(B)** The cellular uptake efficacy of HTCP-Au and HTCP-Au/shNC detected by FCM after incubation at the indicated time points; **(C)** The cellular distribution images of HTCP-Au and HTCP-Au/shNC assayed by CLSM after incubation for 6 h. The scale bar is 50 μm .

3.3. HTCP-Au cytotoxicity and cellular uptake

The MTT assay was performed to evaluate HTCP-Au cytotoxicity in breast cancer 4T1 cells. The cell proliferation rate somewhat decreased with increasing HTCP-Au concentration, but it was over 90% at the highest concentration of 100 $\mu\text{g/ml}$, and similar trends were also found with HTCP-Au/shNC (Fig. 3A). The HTCP-Au vector had no significant cytotoxicity. Next, we investigated the cellular uptake of HTCP-Au on 4T1 cells by using a fluorescent probe, FITC. The cellular uptake efficiency of HTCP-Au and HTCP-Au/shNC increased with time and both exceeded 90%, which indicated that HTCP-Au had a strong cell uptake capacity, with or without DNA loading (Fig. 3B). The subcellular distribution of HTCP-Au was measured by staining lysosomes and nuclei with LysoRed and DAPI, respectively. The HTCP-Au and HTCP-Au/shNC were localized mainly in the cytoplasm (Fig. 3C).

3.4. *In vitro* HTCP-Au/SHPD-L1/DOX antitumor activity

Many studies have shown that AuNPs can be used as a direct anti-tumor weapon, which is due to its good photothermal conversion activity. For example, a hybrid nanostructure with AuNPs layer showed excellent near infrared absorbance and strong temperature elevation, which caused a significant growth inhibitory effect *in vitro* [37]. As for HTCP-Au/shPD-L1/DOX nanoparticles in this study, the 808 nm laser irradiation could induce an increase in cell temperature and showed a time-, dose-, and intensity-dependence, which was consistent with previous report. Based on an overall analysis of photothermal conversion efficiency, economic cost, and clinical demand, we decided that the concentration of HTCP-Au/shPD-L1/DOX at 25 $\mu\text{g/ml}$

and 808 nm laser irradiation for 60 s at 1.5 W/cm² was most appropriate for further *in vitro* experiments on 4T1 cells. The inhibitory rate of HTCP-Au/shPD-L1/DOX with irradiation on 4T1 cells was 89.37% \pm 3.64%, far higher than that of HTCP-Au/shPD-L1 (26.87% \pm 0.77%), HTCP-Au/shNC/DOX (44.87% \pm 2.36%), and HTCP-Au/shNC with irradiation (26.07% \pm 5.58%) (Fig. 4B).

The silencing efficiency of the PD-L1-targeted RNAi was evaluated by qPCR at 48 h post transfection. The cellular expression of PD-L1 mRNA decreased to 23.18% \pm 12.74% in the combined treatment group, which was similar to that of the genetic immunotherapy, but significantly lower than that of the chemotherapy and phototherapy groups (Fig. 4C). Therefore, the combination therapy significantly improved *in vitro* antitumor efficacy and inhibited cellular PD-L1 mRNA expression. We detected the influence of HTCP-Au/shPD-L1/DOX on cell cycle and apoptosis by FCM (Fig. 4D). For HTCP-Au/shPD-L1/DOX with irradiation, the cell cycle was arrested in the S phase, and the percentage of apoptotic cells was far higher than the other groups. Therefore, the results of the *in vitro* experiment indicated that HTCP-Au/shPD-L1/DOX with 808 nm laser irradiation has good antitumor activity on 4T1 cells *in vitro*, benefitting from knockdown of PD-L1, and apoptosis-associated cell death.

3.5. *In vivo* biodistribution and photothermal effect

We used IR783 as a fluorescence marker to clarify HTCP-Au/shNC distribution in 4T1 tumor-bearing mice. The fluorescence intensity in mice increased first and then decreased over time (Fig. 5A). Twenty-four hours after tail vein injection, the significant fluorescence signals of HTCP-Au/shNC-IR783 were concentrated in the tumor tissues, while no obvious fluorescent signals were observed in the IR783

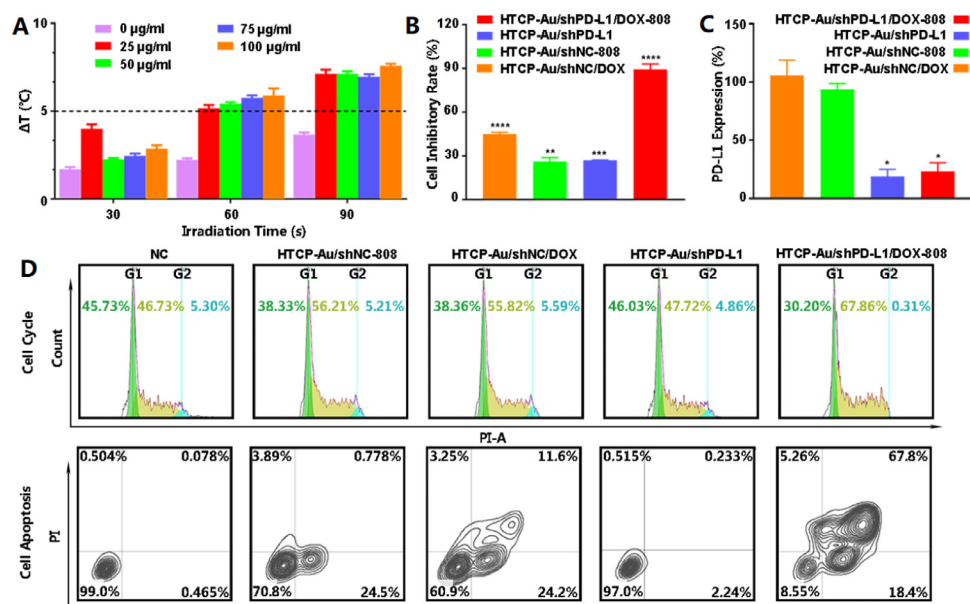


Fig. 4 – Anti-tumor activity on 4T1 cells in vitro. (A) The temperature changes of 4T1 cells treated with different concentrations of HTCP-Au/shPD-L1/DOX after irradiation by 808 nm laser (1.5 W) for various time durations; (B) The cytotoxicity, (C) the PD-L1 mRNA expression and (D) cell cycle and cell apoptosis of 4T1 cells after various treatments for 48 h at the equivalent dose of 25 μ g HTCP-Au/ml, 8.33 μ g shPD-L1/ml, and 10 μ g DOX/ml. Results are shown as mean \pm SD ($n = 5$; * $P < 0.05$; ** $P < 0.01$; * $P < 0.001$; **** $P < 0.0001$).**

control group. The results demonstrated that HTCP-Au/shNC-IR783 travelled in the blood vessels to the tumor rather than to the other organs, and the clearance of HTCP-Au/shNC-IR783 was delayed, compared to IR783 alone. Elevated fluorescence signals aggregated in the tumor tissues of the HTCP-Au/shNC-IR783 group in *ex vivo* imaging, which was consistent with the results of *in vivo* imaging and also confirmed the long circulation and tumor targeting ability of HTCP-Au/shNC (Fig. 5B and S2). These results further confirmed the advantage of long circulation *in vivo* of core-shell nanoparticles, which may be mainly due to the exposed HA shell.

To further investigate the photothermal conversion activity *in vivo*, we irradiated the tumors with a 1.5 W, 808 nm laser. Considering the appropriate accumulation point based on the results of *in vivo* biodistribution, laser irradiation was performed at 5 h post injection of HTCP-Au/shNC. The temperature of the tumor sites increased significantly with the increase in laser irradiation time, regardless of *in situ* tumor injection or tail vein injection (Fig. S3). Considering the temperature requirement of clinical phototherapy, the appropriate laser irradiation time was set to 30 s for HTCP-Au mediated photothermal antitumor therapy. The maximum tumor temperature was 41.4 °C after 30 s irradiation (Fig. 5C).

3.6. *In vivo* HTCP-Au/SHPD-L1/DOX antitumor activity

In recent years, localized treatments have been used to enhance PD-L1 blockade therapy, with good results. Nanomicelles loaded with DOX and immune adjuvants can induce ICD and significantly enhance the anti-tumor and metastasis inhibitory effects of PD-L1-based therapy [22]. Combined genome editing of PD-L1 and photothermal

therapy mediated by AuNPs could reprogram the tumor microenvironment, and show excellent tumor-suppressive effects against primary and metastatic tumors. In this study, we realized the combination therapy of phototherapy, chemotherapy and immune gene therapy through a combined drug delivery system, and investigated the anti-tumor activity of HTCP-Au/shPD-L1/DOX. During the drug administration period, tumor volumes visibly increased over time and differed substantially among groups (Fig. 6A). The mice were sacrificed, and their tumor tissues were excised to calculate the inhibition rates (Fig. 6B and 6C). Compared with the normal saline group (NC), the genetic immunotherapy (HTCP-Au/shPD-L1), chemotherapy (HTCP-Au/shNC/DOX), and phototherapy groups (HTCP-Au/shNC-808) displayed a moderate tumor growth inhibitory rate of 27.75% \pm 6.17%, 25.74% \pm 3.11%, and 30.84% \pm 10.43%, respectively. The tumor inhibition rates were further increased by combining two methods (Fig. S4). As expected, a marked increase of 89.29% \pm 2.80% in tumor growth inhibition was found in the combined treatment group (HTCP-Au/shPD-L1/DOX-808). These results indicate that HTCP-Au is an outstanding drug carrier and HTCP-Au/shPD-L1/DOX can induce a satisfactory antitumor effect.

Next, hematoxylin-eosin (HE) staining of pathological sections was used to delineate the effect of the drug administration systems on mouse tumor cells. The tumor cells in the NC and vector (HTCP-Au/shNC) groups had normal shapes and a compact distribution while the tumor cells in the treatment groups underwent varying degrees of cavitation and nuclear shrinkage (Fig. 6D and S5). In contrast, the most serious damage to the breast tumor tissue was found in the HTCP-Au/shPD-L1/DOX-808 group, which was provided

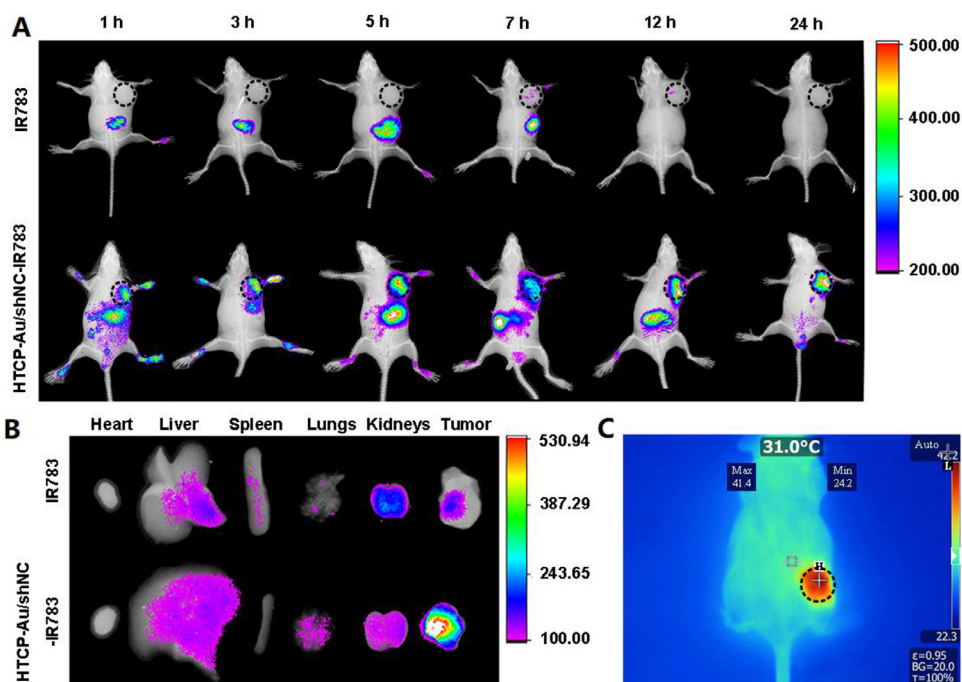


Fig. 5 – Biodistribution and thermal imaging in vivo. (A) In vivo imaging of 4T1 tumor-bearing BALB/c mice at indicated time points after tail vein injection; **(B)** The major organs imaging after treatment for 24 h; **(C)** The thermal imaging in vivo. Black circled area is the site of tumor.

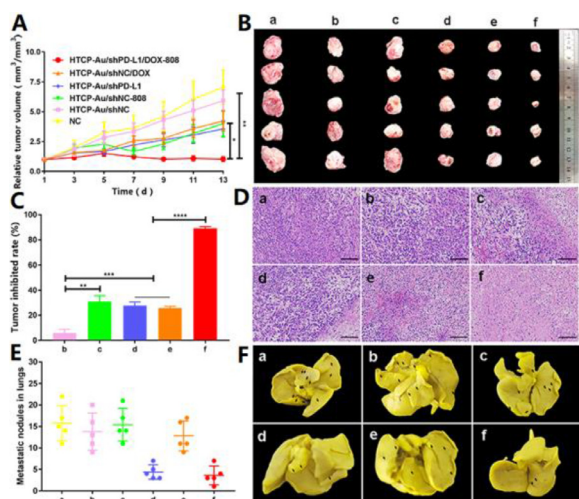


Fig. 6 – Anti-tumor activity on 4T1 tumor-bearing BALB/c mice after various treatments for 12 d (a: normal saline, b: HTCP-Au/shNC, c: HTCP-Au/shNC with 808 nm laser irradiation, d: HTCP-Au/shPD-L1, e: HTCP-Au/shNC/DOX, f: HTCP-Au/shPD-L1/DOX with 808 nm laser irradiation). (A) Relative tumor volume change curves; **(B)** Representative photographs of tumor tissues; **(C)** The tumor growth inhibitory rate; **(D)** HE-stained tumor tissues. The scale bar is 100 μm ; **(E)** The tumor nodules in lungs. Results are shown as mean \pm SD ($n = 5$; * $P < 0.05$; ** $P < 0.01$; *** $P < 0.001$; **** $P < 0.0001$).

synergistic immunotherapy, chemotherapy, and phototherapy under 808 nm laser irradiation, which significantly enhanced antitumor activity in vivo. We also evaluated metastasis inhibition by counting the lung metastases (Fig. 6E and S6). The HTCP-Au/shPD-L1/DOX group with NIR showed the lowest number of tumor nodes, with a fold decrease compared with the NC group, indicating the inhibition of tumor metastasis, which embodied the unique advantages of enhanced immunotherapy.

Subsequently, we further detected the expression of PD-L1 in tumor tissues by qPCR and western blot (Fig. 7A and 7B). In the case of the HTCP-Au/shNC/DOX group, a marked increase in PD-L1 mRNA and protein expression were observed. It has been reported that DOX can enhance the anti-tumor efficiency and activate the expression of PD-L1 by means of increasing the expression level of IFN- γ [38]. In contrast, in the HTCP-Au/shPD-L1 group, PD-L1 mRNA and protein expression levels decreased significantly by $63.39\% \pm 0.76\%$ and $85.48\% \pm 2.18\%$, respectively. Similar results were also observed in the HTCP-Au/shPD-L1/DOX group with 808 nm laser irradiation, and the inhibition rates were $62.61\% \pm 8.02\%$ in mRNA level and $77.05\% \pm 0.33\%$ in protein level.

To investigate the immune activation of HTCP-Au/shPD-L1/DOX, the expression of IFN- γ was considered [4,5]. Induction of ICD can increase the secretion of IFN- γ , which is beneficial for the activation of antigen-presenting cells and improvement in the tumor therapeutic effect [39]. There was an increase in the expression of IFN- γ in all treatment groups to varying degrees (Fig. 7C). In particularly, HTCP-Au/shPD-L1/DOX-808 treatment promoted the expression of IFN- γ most, indicating stimulation of the immune system.

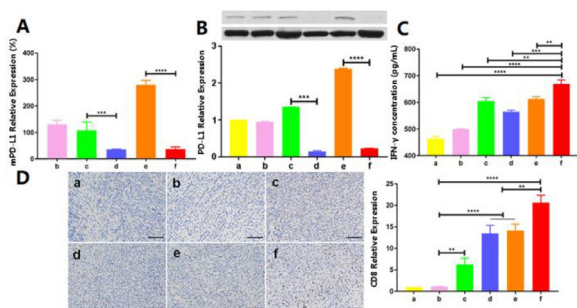


Fig. 7 – Anti-tumor mechanism on 4T1 tumor-bearing BALB/c mice after various treatments for 12 d (a: normal saline, b: HTCP-Au/shNC, c: HTCP-Au/shNC with 808 nm laser irradiation, d: HTCP-Au/shPD-L1, e: HTCP-Au/shNC/DOX, f: HTCP-Au/shPD-L1/DOX with 808 nm laser irradiation). The PD-L1 expression at (A) mRNA and (B) protein levels in tumor tissues; (C) The regulation of IFN- γ secretion; (D) IHC results of CD8⁺ T cells in tumor tissues; The scale bar is 100 μ m. Results are shown as mean \pm SD (n = 5; ** P < 0.01; * P < 0.001; **** P < 0.0001).**

The activation of immune response in tumor sites by synergistic therapy will eventually promote the migration of CD8⁺ T cells to tumor sites, thus generating anti-tumor immunity. A recent work show that the degree of CD8⁺ T cell infiltration is essential for antitumor effect *in vivo* and is an important factor affecting the efficacy of immune checkpoint blockade therapy [4]. Therefore, the CD8⁺ T cells infiltration of tumor tissues was detected by immunohistochemistry (IHC) (Fig. 7D). Just as we expected, HTCP-Au/shPD-L1/DOX-808 treatment induced a marked accumulation of CD8⁺ T cells compared to the other groups, indicating the alleviation of tumor microenvironment immunosuppression and the enhancement of antitumor immunoassay activity. Taken together, these results demonstrated that HTCP-Au/shPD-L1/DOX fulfilled the combination of gene-immunotherapy, chemotherapy, and phototherapy, which effectively activated antitumor immunity, inhibited subcutaneous tumor proliferation, and suppressed metastasis.

3.7. HTCP-Au/shPD-L1/DOX biocompatibility

Reducing systemic toxicity is one of the main purposes of constructing a drug delivery system, so we evaluated the biosafety of the combination therapy of the HTCP-Au/shPD-L1/DOX nano-system in animal experiments. The average body weight of mice in each group increased over time (Fig. 8A and S7). Compared with the NC group, the weight of mice in the free drug DOX group was significantly reduced, showing significant toxicity *in vivo*, which was consistent with reports in the literature [35,36]. In contrast, when DOX was loaded by the core-shell nano-vector, HTCP-Au, to construct HTCP-Au/shNC/DOX and HTCP-Au/shPD-L1/DOX, the body weight of mice in both groups was significantly increased and closely matched that of the NC group. This proved initially that HTCP-Au-based drug delivery systems are conducive to reducing potential systemic toxicity as well as enhancing antitumor activity.

It is well known that the *in vivo* toxicity of DOX mainly manifests as cardiotoxicity, and the toxicity can be greatly reduced by a reasonably designed drug delivery system. Therefore, we verified the biosecurity of HTCP-Au/shPD-L1/DOX by myocardial enzyme spectroscopy (Fig. 8B and S8). Compared with the NC group, the serum aspartate aminotransferase (AST), lactate dehydrogenase (LDH), and creatine kinase (CK) expression levels of the DOX group were significantly increased, while there was no significant change in that of the target group (HTCP-Au/shPD-L1/DOX) with laser irradiation. Similar trends were also found in the mouse organ index experiments and histologic assessments of major organs. There was no obvious difference in the visceral index of other groups except in the heart index of the DOX group (Fig. S9). Consistently, some typical pathological changes, including mild myocardial fiber rupture and renal wall thickening, were obvious in the DOX group, but not in HTCP-Au-based groups, and especially not in the combination treatment group of HTCP-Au/shPD-L1/DOX with laser irradiation. And in the lung tissue sections, groups that involved immunotherapy improved significantly compared to the other groups with a large number of metastases. (Fig. 7C and S10). Therefore, we concluded that the multi-drugs co-delivery system can effectively reduce chemotherapy drug toxicity and provides good biological safety.

4. Conclusion

In this study, we designed a novel core-shell nano drug delivery system based on HTCP-Au/shPD-L1/DOX to spatiotemporally co-deliver different kinds of drugs, which is important in achieving the promising combination of tumor-targeting genetic immunotherapy, chemotherapy, and phototherapy. HTCP-Au/shPD-L1/DOX is characterized by a core of PEI/shPD-L1, a shell of polysaccharide HA for tumor targeting, an intermediate layer of self-assembled alkyl bridge chains for housing DOX, and an additional ornament of AuNPs. HTCP-Au/shPD-L1/DOX had good photothermic activity and high transfection efficiency. Under 808 nm laser irradiation, HTCP-Au/shPD-L1/DOX showed not only high anti-tumor activity by stimulation of the immune system, but also low toxicity. Therefore, the core-shell drug delivery system provides a promising combined therapeutic strategy, yet the synergistic effect mechanism will be further studied.

Conflicts of interest

The authors report no conflicts of interest. The authors alone are responsible for the content and writing of this article.

Acknowledgements

This study was supported by a grant from the National Natural Science Foundation of China (No. 81874394), the Key Science and Technology Research Project of Henan Province of China (No. 202102310150), and the Key Scientific Research Project

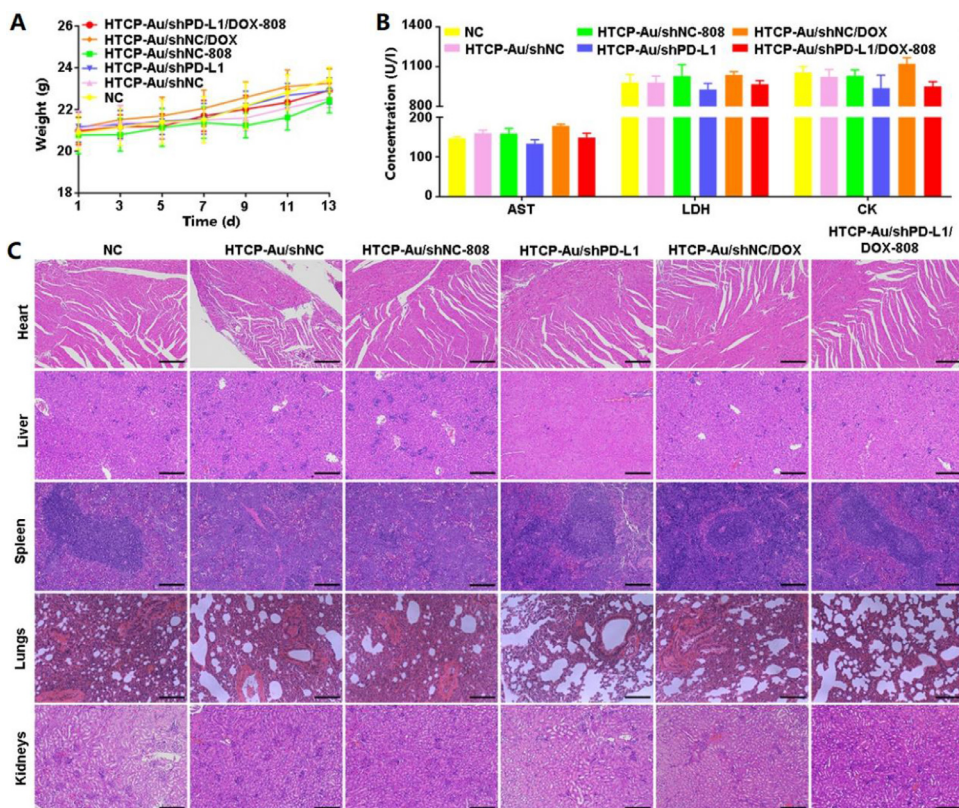


Fig. 8 – Toxicity on 4T1 tumor-bearing BALB/c mice with various treatments in vivo. (A) Body weight changes of 4T1 cells-bearing mice; (B) The regulations of serum myocardial enzyme spectrum in mice; (C) HE stained major organs harvested from mice. The scale bar is 100 μm .

in Colleges and Universities of Henan Province of China (19B350009).

Supplementary materials

Supplementary material associated with this article can be found, in the online version, at doi:10.1016/j.ajps.2021.07.004.

REFERENCES

- [1] Xiao R, Mansour AG, Huang W, Chrislip LA, Wilkins RK, Queen NJ, et al. Adipocytes: a novel target for IL-15/IL-15R alpha cancer gene therapy. *Mol Ther* 2019;27(5):922–32.
- [2] Wu J, Chen J, Feng Y, Zhang S, Shi Z, Lin L, et al. An immune cocktail therapy to realize multiple boosting of the cancer-immunity cycle by combination of drug/gene delivery nanoparticles. *Sci Adv* 2020;6(40):154–63.
- [3] Hewitt SL, Bailey D, Zielinski J, Apte A, Musenge F, Karp R, et al. Intratumoral IL12 mRNA therapy promotes TH1 transformation of the tumor microenvironment. *Clin Cancer Res* 2020;26(23):6284–98.
- [4] Lu J, Liu X, Liao YP, Wang X, Ahmed A, Jiang W, et al. Breast cancer chemo-immunotherapy through liposomal delivery of an immunogenic cell death stimulus plus interference in the IDO-1 pathway. *ACS Nano* 2018;12(11):11041–61.
- [5] Kuai R, Yuan W, Son S, Nam J, Xu Y, Fan Y, et al. Elimination of established tumors with nanodisc-based combination chemoimmunotherapy. *Sci Adv* 2018;4(4):eaao1736.
- [6] Pfrschke C, Engblom C, Rickelt S, Cortez-Retamozo V, Garris C, Pucci F, et al. Immunogenic chemotherapy sensitizes tumors to checkpoint blockade therapy. *Immunity* 2016;44(2):343–54.
- [7] Lu J, Liu X, Liao YP, Salazar F, Sun B, Jiang W, et al. Nano-enabled pancreas cancer immunotherapy using immunogenic cell death and reversing immunosuppression. *Nat Commun* 2017;8:1811.
- [8] Zhou F, Yang J, Zhang Y, Liu M, Lang ML, Li M, et al. Local phototherapy synergizes with immunoadjuvant for treatment of pancreatic cancer through induced immunogenic tumor vaccine. *Clin Cancer Res* 2018;24(21):5335–46.
- [9] Sweeney EE, Cano-Mejia J, Fernandes R. Photothermal therapy generates a thermal window of immunogenic cell death in neuroblastoma. *Small* 2018;14(20):e1800678.
- [10] Ng CW, Li J, Pu K. Recent progresses in phototherapy-synergized cancer immunotherapy. *Adv Funct Mater* 2018;28(46):1840688.
- [11] Duan X, Chan C, Lin W. Nanoparticle-mediated immunogenic cell death enables and potentiates cancer immunotherapy. *Angew Chem Int Ed* 2019;58(3):670–80.
- [12] Kim S, Moon MJ, Poilil Surendran S, Jeong YY. Biomedical applications of hyaluronic acid-based nanomaterials in hyperthermic cancer therapy. *Pharmaceutics* 2019;11(7):306.
- [13] Zhang X, Wu Y, Li Z, Wang W, Wu Y, Pan D, et al. Glycodendron/pyropheophorbide-a

- (Ppa)-functionalized hyaluronic acid as a nanosystem for tumor photodynamic therapy. *Carbohydr Polym* 2020;247:116749.
- [14] Han LF, Hu LJ, Liu FL, Wang X, Huang XX, Liu BW, et al. Redox-sensitive micelles for targeted intracellular delivery and combination chemotherapy of paclitaxel and all-trans-retinoic acid. *Asian J Pharm Sci* 2019;14(5):531–42.
- [15] Xia Y, Guo M, Xu TT, Li YH, Wang CB, Lin ZF, et al. siRNA-loaded selenium nanoparticle modified with hyaluronic acid for enhanced hepatocellular carcinoma therapy. *Int J Nanomedicine* 2018;13:1539–52.
- [16] Lin LT, Cai MY, Deng SH, Huang WS, Huang JJ, Huang XH, et al. Amelioration of cirrhotic portal hypertension by targeted cyclooxygenase-1 2 siRNA delivery to liver sinusoidal endothelium with polyethylenimine 3 grafted hyaluronic acid. *Nanomedicine* 2017;13(7):2329–39.
- [17] Jin S, Muhammad N, Sun Y, Tan Y, Yuan H, Song D, et al. Multispecific platinum (IV) complex deters breast cancer via interposing inflammation and immunosuppression as an inhibitor of COX-2 and PD-L1. *Angew Chem* 2020;59(51):23313–21.
- [18] Yoo B, Jordan VC, Sheedy P, Billig A, Ross A, Pantazopoulos P, et al. RNAi-mediated PD-L1 inhibition for pancreatic cancer immunotherapy. *Sci Rep* 2019;9(1):4712.
- [19] Li J, Chen L, Xiong Y, Zheng X, Xie Q, Zhou Q, et al. Knockdown of PD-L1 in human gastric cancer cells inhibits tumor progression and improves the cytotoxic sensitivity to CIK therapy. *Cell Physiol Biochem* 2017;41(3):907–20.
- [20] Wang L, Ding K, Zheng C, Xiao H, Liu X, Sun L, et al. Detachable nanoparticle-enhanced chemoimmunotherapy based on precise killing of tumor seeds and normalizing the growing soil strategy. *Nano Lett* 2020;20(9):6272–80.
- [21] Hou L, Tian C, Yan Y, Zhang L, Zhang H, Zhang Z. Manganese-based nanoactivator optimizes cancer immunotherapy via enhancing innate immunity. *ACS Nano* 2020;14(4):3927–40.
- [22] Mei L, Liu Y, Rao J, Tang X, Li M, Zhang Z, et al. Enhanced tumor retention effect by click chemistry for improved cancer immunochemotherapy. *ACS Appl Mater Inter* 2018;10(21):17582–93.
- [23] Wen Y, Chen X, Zhu X, Gong Y, Yuan G, Qin X, et al. Photothermal-chemotherapy integrated nanoparticles with tumor microenvironment response enhanced the induction of immunogenic cell death for colorectal cancer efficient treatment. *ACS Appl Mater Inter* 2019;11(46):43393–408.
- [24] Nam J, Son S, Ochyl LJ, Kuai R, Schwendeman A, Moon JJ. Chemo-photothermal therapy combination elicits anti-tumor immunity against advanced metastatic cancer. *Nat Commun* 2018;9:1074.
- [25] Gajendiran M, Rhee JS, Kim K. Recent developments in thiolated polymeric hydrogels for tissue engineering applications. *Tissue Eng Part B Rev* 2018;24(1):66–74.
- [26] Wang Y, Yang CX, Yan XP. Hydrothermal and biomimetalization synthesis of a dual-modal nanoprobe for targeted near-infrared persistent luminescence and magnetic resonance imaging. *Nanoscale* 2017;9(26):9049–55.
- [27] Gřundělová L, Gregorova A, Mráček A, Vícha R, Smolka P, Minařík A. Viscoelastic and mechanical properties of hyaluronan films and hydrogels modified by carbodiimide. *Carbohydr Polym* 2015;119:142–8.
- [28] Liu X, Gao C, Gu J, Jiang Y, Yang X, Li S, et al. Hyaluronic acid stabilized iodine-containing nanoparticles with Au nanoshell coating for X-ray CT imaging and photothermal therapy of tumors. *ACS Appl Mater Inter* 2016;8(41):27622–31.
- [29] Sivaraman SK, Kumar S, Santhanam V. Monodisperse sub-10 nm gold nanoparticles by reversing the order of addition in Turkevich method - The role of chloroauric acid. *J Colloid Interface Sci* 2011;361(2):543–7.
- [30] Zhao Y, Burkert SC, Tang Y, Sorescu DC, Kapralov AA, Shurin GV, et al. Nano-gold corking and enzymatic uncorking of carbon nanotube cups. *J Am Chem Soc* 2015;137(2):675–84.
- [31] Shi P, Amarnath Praphakar R, Deepa S, Suganya K, Gupta P, Ullah R, et al. A promising drug delivery candidate (CS-g-PMDA-CYS-fused gold nanoparticles) for inhibition of multidrug-resistant uropathogenic *Serratia marcescens*. *Drug Deliv* 2020;27(1):1271–82.
- [32] Akbarinejad A, Hisey CL, Brewster D, Ashraf J, Chang V, Sabet S, et al. Novel electrochemically switchable, flexible, microporous cloth that selectively captures, releases, and concentrates intact extracellular vesicles. *ACS Appl Mater Inter* 2020;12(35):39005–13.
- [33] Duan R, Zhou X, Xing D. Electrochemiluminescence biobarcode method based on cysteamine-gold nanoparticle conjugates. *Anal Chem* 2010;82(8):3099–103.
- [34] Ren XL, Liu L, Zhou YX, Zhu Y, Zhang H, Zhang ZZ, et al. Nanoparticle siRNA against BMI-1 with a polyethylenimine-laminarin conjugate for gene therapy in human breast cancer. *Bioconjug Chem* 2016;27(1):66–73.
- [35] Pérez-Arnaiz C, Busto N, Leal JM, García B. New insights into the mechanism of the DNA/doxorubicin interaction. *J Phys Chem B* 2014;118(5):1288–95.
- [36] Fan XS, Luo Z, Ye NY, You ML, Liu MT, Yun Y, et al. AuNPs decorated PLA stereocomplex micelles for synergetic photothermal and chemotherapy. *Macromol Biosci* 2021:2100062.
- [37] Nan XY, Zhang XJ, Liu YQ, Zhou MJ, Chen XF, Zhang XH. Dual-targeted multifunctional nanoparticles for magnetic resonance imaging guided cancer diagnosis and therapy. *ACS Appl Mater Inter* 2017;9(11):9986–95.
- [38] Gao F, Zhang C, Qiu WX, Dong X, Zheng DW, Wu W, et al. PD-1 blockade for improving the antitumor efficiency of polymer-doxorubicin nanoprodrug. *Small* 2018;14(37):e1802403.
- [39] Hein KM, Ros W, Kok M, Steeghs N, Beijnen JH, Schellens JHM. Enhancing anti-tumor response by combining immune checkpoint inhibitors with chemotherapy in solid tumors. *Ann Oncol* 2019;30(2):219–35.